2.E:2.N

Nuclear Physics **A270** (1976) 236–254;

THE REAL PART OF THE NUCLEUS-NUCLEUS INTERACTION

Fl. STANCU †

University of Oxford, Nuclear Physics Department, Keble Road, Oxford

and

Université de Liège, Institut de Physique, Sart Tilman, B-4000 Liège 1, Belgium

and

D. M. BRINK

University of Oxford, Theoretical Physics Department, 12 Parks Road, Oxford

Received 15 December 1975
(Revised 7 May 1976)

Abstract: The real part of the interaction potential for several pairs of magic nuclei has been derived from the Skyrme interaction density functional. The matter density of each nucleus is described by a Fermi distribution adjusted to reproduce the Skyrme-Hartree-Fock densities. Exchange effects due to antisymmetrization are taken into account in an approximate way. The tail of the resulting potential can be accurately approximated with a Woods-Saxon shape beyond the inflexion point of the calculated potential. The parameters of these Woods-Saxon potentials show regularities with respect to the masses of the target and projectile. We have tested the validity of the real part of the potential against elastic scattering data by choosing an imaginary part with the same geometry and a variable strength. For the energy range we consider the calculated grazing angles are somewhat larger than the experimental ones.

1. Introduction

In the last few years various attempts have been made to derive the real part of the interaction potential between two heavy ions starting from an effective two-body interaction. The simplest approach is to fold the effective nucleon-nucleon interaction into the densities of both nuclei. The densities are constructed from shell-model wave functions or obtained from electron scattering data. A critical review of this double folding together with the simple folding [1]) has been made recently by Satchler [2]). Although these models can predict the qualitative features of the elastic scattering data, a renormalization of the strength of the real potential to about one-half of its value at the strong absorption radius is necessary in order to obtain quantitative agreement [2]). Possible reasons for the discrepancy could be the neglect of the saturation effects or exchange effects due to antisymmetrization.

A direct way to take saturation effects into account is to derive a folded potential from a density dependent effective interaction [3,4]). It has been shown explicitly [3])

† Chercheur IISN.

that the density dependent part of the two-nucleon interaction tends to diminish the attraction brought in by the density independent part. Such a result is consistent with the need to renormalize the folded potentials derived from density independent interactions [2]).

Although not based directly on an effective interaction, a further step in the calculation of the nucleus-nucleus potential was made by using the energy density formalism of Brueckner [5]). In this framework the effect of the repulsive core and the Pauli principle are taken into account in some average way. With one exception [6]) the applications of the Brueckner energy density formalism use the so called "sudden approximation" where the density of the composite system is given by the sum of densities of individual nuclei at all distances. It is expected that for distances where the Pauli principle plays a less important role the potential derived within the sudden approximation should have the right order of magnitude. Indeed, Ngô *et al.* [7]) have shown that such a potential is able to reproduce the experimentally known interaction barrier for a large number of projectiles and targets.

At present the most sophisticated microscopic derivation of the real part of the nucleus-nucleus optical potential is based on self-consistent Hartree-Fock calculations [8]). These calculations include both the exchange and the saturation effects. They provide an adiabatic limit of the interaction potential which corresponds to low energy collisions, where the nuclei have time to readjust themselves to the density of the nuclear matter. Unfortunately numerical difficulties prevent the extension of these calculations to systems heavier than $^{16}O+^{16}O$.

In a previous paper [9]) we have used the energy functional of the Skyrme density-dependent interaction [10]) to derive the real part of the interaction potential between two ^{16}O nuclei. Such an approach is very similar to the Brueckner energy density formalism [5]). Ingredients of our method were the Skyrme interaction parameters and the densities of the composite system and the separated nuclei. The effect of the saturation properties of nuclear forces was included by using Skyrme interaction parameters derived from Hartree-Fock calculations which fit binding energies of finite nuclei. Calculations were performed with the sets SI and SII provided by ref. [10]) and the dependence on different parametrizations was discussed. We also made a detailed analysis of the exchange effects due to antisymmetrization. The ground state of the composite system was described by a Slater determinant built from harmonic oscillator wave functions centered at two different points separated by a distance R. It was shown explicitly that the exchange effects due to antisymmetrization are important at any distance R and it was found that they come mainly through the modifications produced by antisymmetrization on the kinetic energy density. This result suggested a way of estimating the exchange effects by making the Thomas-Fermi approximation for the kinetic energy of the composite system. It was shown that this approximation accounts for over 75 % of the exchange effects for separations R larger than twice the rms radius of ^{16}O but it overestimates the exchange effects by $\approx$ 20 % at the barrier.

In the present paper we extend the formalism used in ref. [9]) to the calculation of the real part of the interaction potential between any combination of two closed-shell nuclei as ^{16}O, ^{40}Ca, ^{48}Ca, ^{56}Ni, ^{90}Zr and ^{208}Pb. We use the approximation discussed in ref. [9]) to include the effects due to antisymmetrization and take more realistic nuclear densities related to those resulting from Skyrme-Hartree-Fock calculations [11,12]). Moreover the set SIII of the Skyrme interaction parameters used here provides a better description of nuclear properties than SI and SII and it has a large domain of applicability over the whole periodic table [11]).

In the following section we briefly describe the formalism and discuss the approximations used for the densities. In sect. 3 we exhibit the results. We parametrize the tail of the calculated potential with a Woods-Saxon shape and discuss the dependence of the parameters on the masses of nuclei involved. A comparison with the work of Ngô *et al.* [7]) based on Brueckner formalism is also made. In sect. 4 we calculate the elastic scattering cross section for some pairs of nuclei choosing an imaginary part of the potential with one free parameter and compare with elastic scattering data at several energies. In sect. 5 we present the conclusions.

2. The formalism

We are looking for an interaction potential V as a function of the separation distance R between the centres of the interacting nuclei. We define V as the difference between the energy expectation value E of the whole system calculated at a finite distance R and at infinity, i.e. at a distance where the two nuclei are completely separated,

$$V(R) = E(R) - E(\infty). \tag{1}$$

The expectation value E is given by the energy functional of the Skyrme interaction derived for a system whose ground state is described by a Slater determinant [10]). The quantity E is expressed as a volume integral,

$$E = \int H(\boldsymbol{r})\mathrm{d}\boldsymbol{r}, \tag{2}$$

over the energy density $H(\boldsymbol{r})$ which is an algebraic function of the nucleon densities ρ_n, ρ_p, $\rho = \rho_n + \rho_p$, kinetic energy densities τ_n, τ_p, $\tau = \tau_n + \tau_p$ and spin densities $\boldsymbol{J}_n$, $\boldsymbol{J}_p$, $\boldsymbol{J} = \boldsymbol{J}_n + \boldsymbol{J}_p$ if time reversal invariance is assumed [13]). For spin-saturated nuclei the energy density $H(\boldsymbol{r}) = H(\rho, \tau)$ has the following expression:

$$H(\rho,\tau) = \frac{\hbar^2}{2m}\tau + \tfrac{1}{2}t_0[(1+\tfrac{1}{2}x_0)\rho^2 - (x_0+\tfrac{1}{2})(\rho_n^2+\rho_p^2)] + \tfrac{1}{4}(t_1+t_2)\rho\tau$$
$$+\tfrac{1}{8}(t_2-t_1)(\rho_n\tau_n+\rho_p\tau_p) + \tfrac{1}{16}(t_2-3t_1)\rho\nabla^2\rho + \tfrac{1}{32}(3t_1+t_2)(\rho_n\nabla^2\rho_n+\rho_p\nabla^2\rho_p) + \tfrac{1}{4}t_3\rho_n\rho_p\rho. \tag{3}$$

Here the term containing the Coulomb interaction has been ignored. Then the potential (1) is calculated by performing the integral

$$V(R) = \int [H(\rho,\tau) - H(\rho_1,\tau_1) - H(\rho_2,\tau_2)]\mathrm{d}\boldsymbol{r}, \tag{4}$$

where 1 and 2 refer to the separated nuclei. The Skyrme interaction parameters x_0, t_0, t_1, t_2 and t_3 we are using here is the set SIII from ref. [11]). They are given in table 1. According to ref. [11]) the set SIII gives a remarkable agreement with the

TABLE 1

Parameters of the Skyrme interaction SIII [a])

t_0 (MeV · fm^3)	t_1 (MeV · fm^5)	t_2 (MeV · fm^5)	t_3 (MeV · fm^6)	x_0
−1128.75	395.0	−95.0	14000.0	0.45

[a]) Ref. [11]).

experimental total binding energies of magic nuclei. It also gives single particle level spectra and charge densities in reasonable good agreement with the experimental data. It was suggested that the deviation found between the calculated and experimental electron scattering cross section is due to the fact that the Hartree-Fock density obtained with the set SIII has a surface thickness smaller than one finds from the experimental density.

At present it is impossible to make self-consistent calculations for pairs of nuclei much heavier than ^{16}O; but some variational calculations [14]) show that, for distances larger than the sum of the rms radii of the interacting nuclei, effects due to distortion of single particle wave functions are not important. We therefore expect that our results should not be too different from those of variational calculations for such separations.

The calculations of the potential $V(R)$ from eq. (4) involves the knowledge of the densities ρ and τ of the composite system and of the separated nuclei ρ_i and τ_i ($i = 1, 2$). By using the approximations (5) and (6) for the densities we reduce the problem to the knowledge of the densities of the separated nuclei as a function of R. In this way we can perform simple calculations and include in the same time the major part of the exchange effect due to antisymmetrization.

According to ref. [9]) we can include over 75 % of the exchange effects due to antisymmetrization for distances larger than the sum of rms radii of interacting nuclei by taking (q = n, p)

$$\rho_q = \rho_{1q} + \rho_{2q}, \tag{5}$$

$$\tau_q' \approx \tau_q^{\mathrm{TF}} = \tfrac{3}{5}(3\pi^2)^{\frac{2}{3}}(\rho_{1q}+\rho_{2q})^{5/3}. \tag{6}$$

The Thomas-Fermi approximation is also used of the kinetic energy density of the individual nuclei

$$\tau'_{iq} \approx \tau^{TF}_{iq} = \tfrac{3}{5}(3\pi^2)^{\frac{2}{3}}(\rho_{iq})^{5/3} \qquad (i = 1, 2;\ q = \text{n, p}). \tag{7}$$

The formulae (6) and (7) are used to approximate the quantity

$$\tau' = -\sum_{\alpha(\text{occ})} \psi^*_\alpha \nabla^2 \psi_\alpha, \tag{8}$$

where the ψ_α are the occupied single particle wave functions, while the energy density (3) is expressed in terms of

$$\tau = \sum_{\alpha(\text{occ})} \nabla\psi^*_\alpha \nabla\psi_\alpha. \tag{9}$$

These two quantities are related through

$$\tau = \tau' + \tfrac{1}{2}\nabla^2\rho. \tag{10}$$

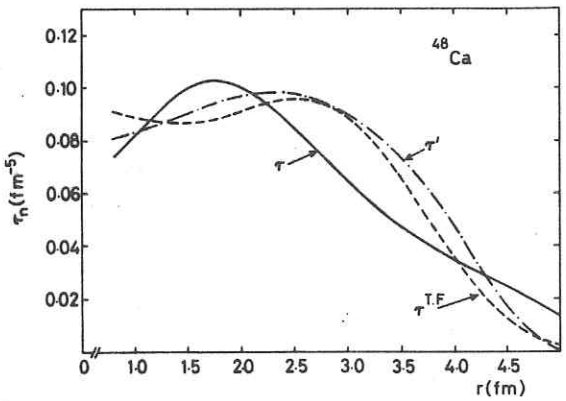

Fig. 1. Neutron kinetic energy density as a function of r for ^{48}Ca. Curves $\tau'(r)$ and $\tau(r)$ are calculated from formulae (8) and (9) respectively by using Hartree-Fock single particle wave functions obtained with the set SIII. The corresponding Hartree-Fock density is used to obtain the Thomas-Fermi approximation (7) plotted as the curve $\tau^{TF}(r)$.

As an example fig. 1 shows τ and τ' calculated from Hartree-Fock neutron single particle wave functions for ^{48}Ca and also τ^{TF} calculated from eq. (7) with the Hartree-Fock density. The comparison shows that τ^{TF} is a better approximation to τ' than it is to τ.

In principle we should use Hartree-Fock densities in eqs. (5)–(7) but for reasons of simplicity we make two further approximations.

First we take

$$\rho_{in} = \frac{N_i}{A_i}\rho_i; \qquad \rho_{ip} = \frac{Z_i}{A_i}\rho_i \qquad (i = 1, 2), \tag{11}$$

where ρ_i is obtained by the addition of calculated [12]) neutron and proton densities. This approximation is quite satisfactory in the surface region but it is less good for regions where the densities are smaller than $10^{-1}\,\rho_0$ (ρ_0 is an average central density). The second approximation is to replace the Hartree-Fock densities ρ_1 and ρ_2 by Fermi-type distributions having radius parameter R_i and surface thickness a which reproduce exactly the Hartree-Fock rms radius $\langle r^2\rangle^{\frac{1}{2}}_{\text{m}}$ and describe the surface region as well as possible. We vary a and find the other parameters R_i and ρ_0 from the normalization conditions

$$R_i^2 = \tfrac{1}{3}[5\langle r^2\rangle_{\text{m}} - 7\pi^2 a^2],$$
$$\rho_0 = \frac{3A}{4\pi R_i^3}\,\frac{1}{1+\pi^2 a^2/R_i^2}. \tag{12}$$

TABLE 2

Parameters of Fermi type distributions which fit Skyrme-Hartree-Fock matter densities [a])

Nucleus	$\langle r^2\rangle^{1/2}_m$	ρ_0	R_i	a
^{16}O	2.6269	0.1607	2.6538	0.44
^{40}Ca	3.3841	0.1577	3.7416	0.47
^{48}Ca	3.5422	0.1600	3.9780	0.47
^{56}Ni	3.6933	0.1605	4.2008	0.47
^{90}Zr	4.2872	0.1533	5.0543	0.47
^{208}Pb	5.5968	0.1482	6.8321	0.49

[a]) From refs. [11,12]).

The values we found for ρ_0, R_i and a, together with the Hartree-Fock result [11,12]) for $\langle r^2\rangle^{\frac{1}{2}}_{\text{m}}$, are presented in table 2 for all nuclei we are interested in. Two examples of this adjustment are given in figs. 2a and b for ^{16}O and ^{40}Ca respectively.

Before presenting the results we would like to indicate how the saturation properties of the Skyrme interaction can influence the behaviour of the nucleus-nucleus potential. For this purpose we ignore the effect of the antisymmetrization on both ρ and τ, i.e. together with the relation (5) we take

$$\tau_q = \tau_{1q} + \tau_{2q} \qquad (q = \text{n, p}), \tag{13}$$

instead of using eq. (6).

We express the integrand of eq. (4) in terms of the average Hartree-Fock potentials U_{iq} [ref. [10])] of the separated nuclei

$$U_{iq} = t_0[(1+\tfrac{1}{2}x_0)\rho_i - (x_0+\tfrac{1}{2})\rho_{iq}] + \tfrac{1}{4}t_3(\rho_i^2 - \rho_{iq}^2)$$
$$-\tfrac{1}{8}(3t_1 - t_2)\nabla^2\rho_i + \tfrac{1}{16}(3t_1+t_2)\nabla^2\rho_{iq} + \tfrac{1}{4}(t_1+t_2)\tau_i + \tfrac{1}{8}(t_2-t_1)\tau_{iq}. \tag{14}$$

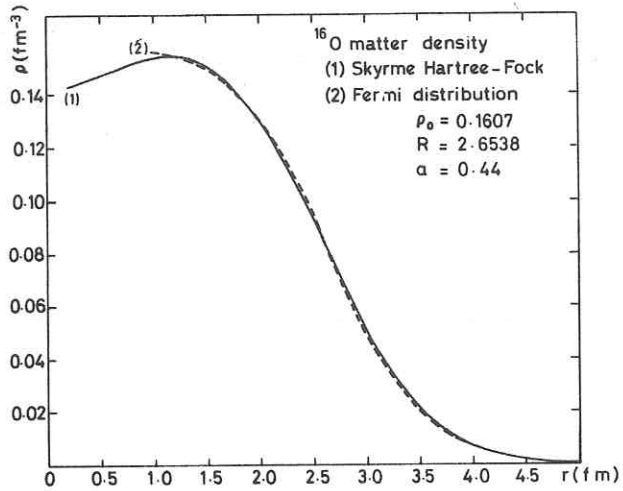

Fig. 2a. Density distribution for ^{16}O. Curve (1) is the Hartree-Fock density $\rho = \rho_n + \rho_p$ of ref. [12]). Curve (2) represents the fit of the Hartree-Fock result with a Fermi type distribution.

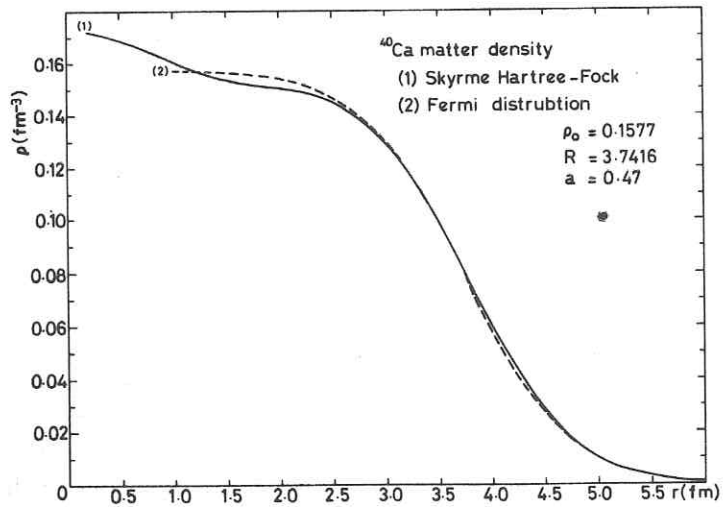

Fig. 2b. Same as 2a, but for ^{40}Ca.

By using this formula and the approximation (11) we obtain

$$H(\rho,\tau)-H(\rho_1,\tau_1)-H(\rho_2,\tau_2) = \frac{1}{2}\left[\left(\frac{N_1}{A_1}U_{2n}+\frac{Z_1}{A_1}U_{2p}\right)\rho_1+\left(\frac{N_2}{A_2}U_{1n}+\frac{Z_2}{A_2}U_{1p}\right)\rho_2\right]$$

$$+\tfrac{1}{8}t_3\left[\left(1-\frac{N_2N_1^2+Z_2Z_1^2}{A_2A_1^2}\right)\rho_2\rho_1^2+\left(1-\frac{N_1N_2^2+Z_1Z_2^2}{A_1A_2^2}\right)\rho_1\rho_2^2\right]$$

$$+\frac{1}{16}\left[(t_2-t_1)\frac{N_1N_2+Z_1Z_2}{A_1A_2}+2(t_2+t_1)\right](\rho_1\tau_2+\rho_2\tau_1). \quad (15)$$

The r.h.s. of eq. (15) has three distinct terms, each of them being symmetric at the interchange of nuclei 1 and 2. The first term is a folding type potential with separate contributions from neutrons and protons. This term produces an attractive, deep potential. The other two terms will compensate for this excessive attraction and this can be seen looking at the values taken by the parameters t_1, t_2 and t_3 (table 1). These parameters are just the strength of the velocity dependent and density dependent terms of the Skyrme interaction required to fit the saturation properties of nuclear matter.

3. Results

By using the formalism of the previous section we have calculated the interaction potential for all possible pairs of magic nuclei listed in table 2. Some examples are drawn in figs. 3a and b. All potentials have a common shape, with a repulsive core at short distances and an attractive part having the minimum centered around a distance equal to the sum of rms radii of interacting nuclei. The repulsive core is essentially a consequence of the lack of distortion in the single particle wave functions and of the approximations we have used for the densities. Variational calculations [8,14]) or the adiabatic treatment of the density [6]) show that the repulsive core disappears when the single particle wave functions or densities are allowed to be distorted. In ref. [9]) we have shown that the radius of the repulsive core depends on the approximation we make for the kinetic energy density. A Thomas-Fermi approximation with an ellipsoidal distribution [9]) in the momentum space brings more repulsion than a spherical one. Although this deformed Thomas-Fermi approximation is better near the minimum of the potential, both spherical and deformed Thomas-Fermi approximations give similar results for the potential around the barrier. Therefore we consider that the use of the spherical Thomas-Fermi formula (6) is satisfactory in finding the tail of the real part of the nucleus-nucleus interaction.

The surface region is the only part of the real potential which is significant for the calculation of the elastic scattering cross section at grazing angles when the process is dominated by strong absorption [2]). For this reason we use only the potential curve beyond its minimum in the following discussion. For practical purposes we found useful to parametrize this part of the potential by a Woods-Saxon shape. We fixed both the range R_V and the depth V_0 of the Woods-Saxon shape by taking $R_V \approx R_0$ and $V_0 = 2V(R_0)$ where R_0 is the inflexion point of the

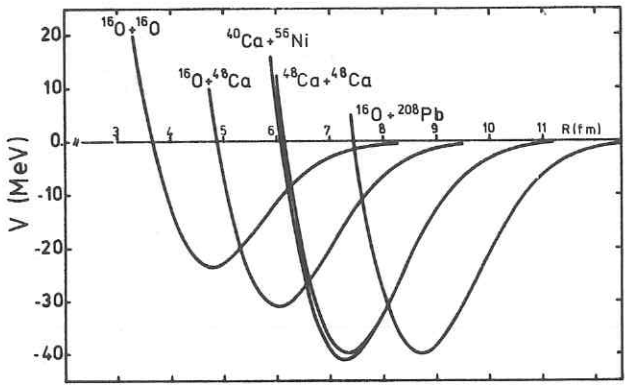

Fig. 3a. Nuclear interaction potential for pairs of magic nuclei as a function of the separation distance R between their centres.

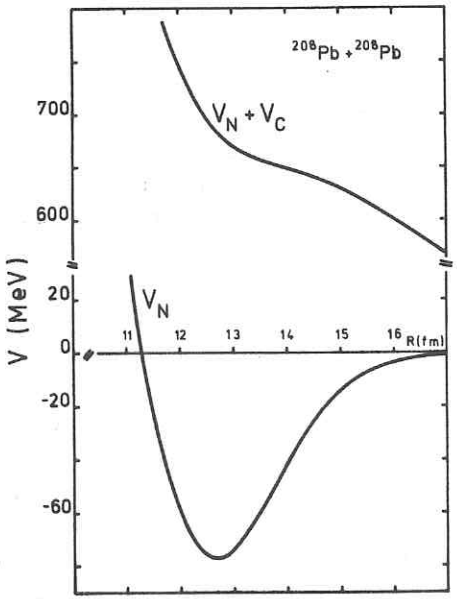

Fig. 3b. Interaction potential between two ^{208}Pb nuclei as a function of R. Here, V_N is the nuclear potential and V_N+V_C is the nuclear plus Coulomb potential.

calculated potential V. The corresponding value for the diffusivity T was found by trying to reproduce accurately the height of the calculated barrier, obtained by adding to the nuclear potential (4) a Coulomb interation of the form $V_C = Z_1 Z_2 e^2/R$. The values found for the Woods-Saxon parameters V_0, R_0 and T corresponding to all possible pairs of magic nuclei ^{16}O, ^{40}Ca, ^{48}Ca, ^{56}Ni, ^{90}Zr and ^{208}Pb are given in table 3. They fit the calculated interaction for distances between the inflexion points R_0 and the barrier R_B with an accuracy better than 1 %. As an example in fig. 4 we

TABLE 3

Parametrization of the tail of the nucleus-nucleus potential with a Woods-Saxon shape

Pair	$A_1^{1/3}+A_2^{1/3}$	$A_1^{2/3}+A_2^{2/3}-(A_1+A_2)^{2/3}$	V_0	R_0	T	V_N	R_B
^{16}O + ^{16}O	5.0397	2.6198	28.03	5.8	0.561	− 0.91	7.7
^{16}O + ^{40}Ca	5.9398	3.4085	35.52	6.85	0.586	− 1.99	8.5
^{16}O + ^{48}Ca	6.1541	3.5573	36.52	7.1	0.582	− 1.86	8.8
^{16}O + ^{56}Ni	6.3457	3.6798	37.92	7.3	0.587	− 2.74	8.8
^{16}O + ^{90}Zr	7.0012	4.0349	41.45	8.10	0.593	− 3.05	9.6
^{16}O + ^{208}Pb	8.4448	4.5716	49.51	9.80	0.62	− 5.40	11.1
^{40}Ca + ^{40}Ca	6.8399	4.8258	48.26	7.85	0.615	− 4.51	9.25
^{40}Ca + ^{48}Ca	7.0542	5.1125	49.89	8.10	0.612	− 3.95	9.6
^{40}Ca + ^{56}Ni	7.2458	5.3674	51.91	8.30	0.618	− 6.52	9.5
^{40}Ca + ^{90}Zr	7.9014	6.1168	57.50	9.1	0.623	− 8.40	10.2
^{40}Ca + ^{208}Pb	9.3449	7.3286	70.16	10.8	0.647	−14.02	11.7
^{48}Ca + ^{48}Ca	7.2685	5.4495	48.97	8.36	0.608	− 3.60	9.9
^{48}Ca + ^{56}Ni	7.4601	5.7298	54.66	8.53	0.618	− 5.37	9.9
^{48}Ca + ^{90}Zr	8.1156	6.5861	57.96	9.35	0.620	− 6.81	10.6
^{48}Ca + ^{208}Pb	9.5592	7.9958	68.01	11.07	0.643	−12.95	12.0
^{56}Ni + ^{56}Ni	7.6517	6.0393	56.01	8.75	0.620	− 8.69	9.8
^{56}Ni + ^{90}Zr	8.3073	6.9933	63.32	9.53	0.63	−11.17	10.5
^{56}Ni + ^{208}Pb	9.7509	8.5897	76.56	11.25	0.65	−20.60	11.9
^{90}Zr + ^{90}Zr	8.9628	8.2862	68.99	10.34	0.632	−14.09	11.2
^{90}Zr + ^{208}Pb	10.4064	10.5739	81.06	12.09	0.642	−28.01	12.5
^{208}Pb + ^{208}Pb	11.8500	14.4846	98.78	13.8	0.66		

The last two columns are the value of the nuclear potential V_N at the barrier and the position R_B of the barrier.

show the fit of the interaction potential between ^{16}O and ^{40}Ca by the Woods-Saxon potential of table 3. In addition in the second column of table 4 we indicate the numerical values taken by the potential at few distances between R_0 and R_B (first column). The third column represents the Woods-Saxon potential of table 3. In the last two columns of the same table we show how the fit deteriorates when T is increased and V_0 and R_0 remain fixed. The difference with respect to the calculated curve is given in percent in brackets. It turns out that a change of ≈ 0.005 in the

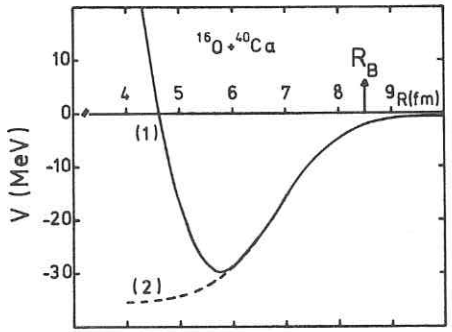

Fig. 4. Interaction potential for ^{16}O + ^{40}Ca as a function of R. Curve (1) is the calculated potential and curve (2) is the Woods-Saxon potential from table 3, and R_B is the position of the Coulomb barrier.

TABLE 4

Interaction potential for $^{16}O+^{40}Ca$ at four values of the separation distance R

R	V	$V^{WS}_{T=0.586}$	$V^{WS}_{T=0.590}$	$V^{WS}_{T=0.635}$
7.0	−15.42	−15.50 (0.52)	−15.51 (0.58)	−15.67 (1.62)
7.5	− 8.74	− 8.81 (0.80)	− 8.86 (0.80)	− 9.39 (7.44)
8.0	− 4.38	− 4.38 (0.00)	− 4.43 (1.14)	− 4.99 (13.93)
8.5	− 1.99	− 2.00 (0.50)	− 2.04 (2.00)	− 2.46 (23.62)

The second column is the calculated potential. The last three columns are Woods-Saxon potentials with same $V_0 = 35.52$ MeV, $R_0 = 6.85$ fm but $T = 0.586$; 0.590 and 0.635 respectively.

diffusivity still reproduces the calculated potential within 2 % error but an increase of 0.05 implies a decrease of ≈ 24 % in the potential at the barrier ($R_B = 8.5$ fm). The percentage change in the potential at the barrier for a change $\delta T = 0.05$ is less than 20 % for heavier pairs of nuclei.

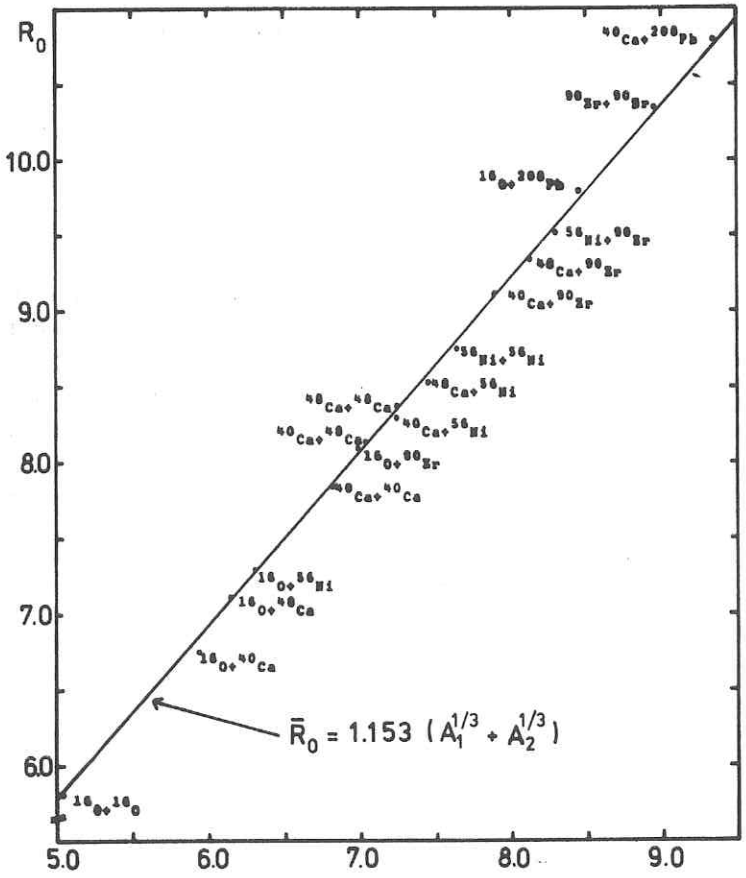

Fig. 5. Plot of the parameter R_0 of table 3 as a function of $A_1^{1/3}+A_2^{1/3}$.

It is interesting to notice some regularities in the dependence of the parameters V_0, R_0 and T of table 3 on the masses A_1 and A_2 of the interacting pair. As fig. 5 shows the parameter R_0 is well approximated by the formula

$$\bar{R}_0 = 1.153(A_1^{\frac{1}{3}}+A_2^{\frac{1}{3}}). \tag{16}$$

As suggested in refs. [15,16]) a convenient way to represent the dependence of V_0 on A_1 and A_2 is a plot it against the quantity $D = A_1^{\frac{2}{3}}+A_2^{\frac{2}{3}}-(A_1+A_2)^{\frac{2}{3}}$. If two nuclei merge adiabatically then their interaction would be represented by a change in surface energy of a liquid drop model. Then the ratio V_0/D should be a constant for all nuclei. Our potential is based on the sudden approximation and consequently has a hard core at the origin. From an adiabatic approach one would expect to get a potential similar to the present one in the tail region where our calculated potentials are well approximated by a Woods-Saxon potential. Near the origin a potential derived from an adiabatic or variational approach should have a shape more similar to a Woods-Saxon potential [14]). Hence we expect that the Woods-Saxon parametrization found here might give a reasonable estimate of the adiabatic

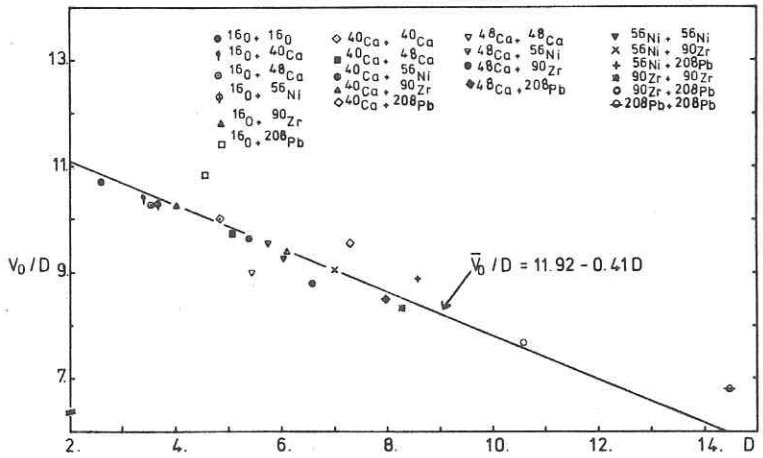

Fig. 6. The dependence of the parameter V_0 of table 3 on $D = A_1^{2/3}+A_2^{2/3}-(A_1+A_2)^{2/3}$.

potential for a wide range of separations between the interacting nuclei. Fig. 6 shows that V_0/D decreases with D and its average dependence on D can be described by the straight line

$$V_0/D = 11.92-0.41D. \tag{17}$$

Such a result represents a deviation in the dependence on D from the predictions of the liquid drop model, but the relation (17) can still be used to estimate V_0 from the mass numbers A_1 and A_2 of a pair of interacting nuclei.

The dependence of T on $A_1^{\frac{1}{3}}+A_2^{\frac{1}{3}}$ is displayed in fig. 7. We find a small average

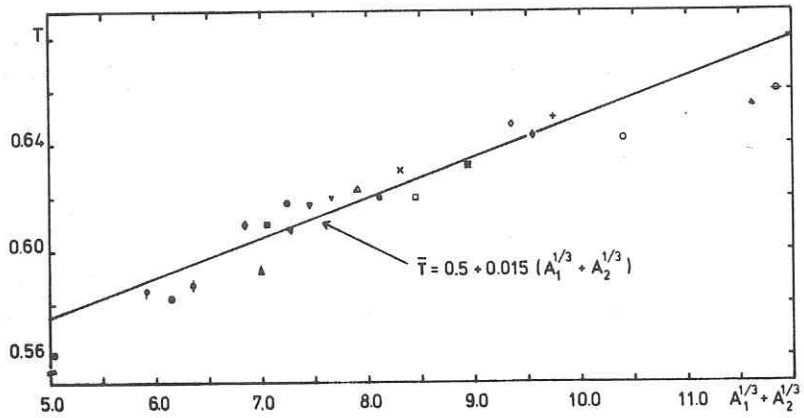

Fig. 7. The dependence of the parameter T of table 3 on $A_1^{1/3}+A_2^{1/3}$. Pairs of nuclei are represented in the same way as in fig. 6.

increase of T with $A_1^{\frac{1}{3}}+A_2^{\frac{1}{3}}$ represented by the line

$$\bar{T} = 0.015(A_1^{\frac{1}{3}}+A_2^{\frac{1}{3}})+0.5. \tag{18}$$

The largest departure from this line is for the $^{16}O+^{16}O$ and $^{208}Pb+^{208}Pb$ systems. In the latter case the parameter T is determined with some ambiguity due to the fact that the interaction V_N+V_C (nuclear + Coulomb) does not have a barrier (fig. 3b). This means that we cannot determine T in the same way as for the other cases, i.e. by trying to reproduce the height of the barrier accurately.

For all the pairs of nuclei in table 3 except $^{208}Pb+^{208}Pb$, eqs. (16), (17) and (18) reproduce values of R_0, V_0 and T in the same table to within 1 %, 8 % and 3 % respectively. Using parameters $\bar{R}_0$, $\bar{V}_0$ and $\bar{T}$ from eqs. (16), (17) and (18) the Woods-Saxon potential gives the potential $V(R)$ calculated from the Skyrme interaction to within 12 % for $R_0 < R < R_B$ except for $^{16}O+^{16}O$ (14 %), $^{16}O+^{208}Pb$ (15 %) and $^{208}Pb+^{208}Pb$ (24 %). This shows that we found difficulties in fitting the lightest and the heaviest systems into the average behaviour. In spite of this, a practical aspect of the regularities found in the parameters V_0, R_0 and T could possibly be the use of formulae (16)–(18) to predict the interaction potential between other pairs of nuclei which are not too far form a spherical shape.

The potentials in ref. [16]) were calculated on the bais of a liquid drop model and, as they have been parametrized by Woods-Saxon shapes, it is possible to make a direct comparison with potentials obtained in the present work. In both cases the parameters have the same order of magnitude. The depth in ref. [16]) is $V_0 = 17\,D$ MeV, i.e. larger than ours. The calculations in our paper also predicts a different dependence on D which cannot be obtained in the crude liquid drop model. The potential radii in ref. [16]) are somewhat smaller than those presented here and this might partly compensate for the larger depth. Perhaps a more significant difference is that the surface diffuseness parameters T obtained in the present work are about 40 % smaller than those given in ref. [16]). In both cases T increases slightly with the masses of the colliding nuclei.

From the experimental point of view an interesting quantity which can be found from our calculations is the height $V_B = V_N+V_C$ and the position R_B of the interaction barrier. The height of the barrier can be determined within few MeV from threshold energy measurements. From the large body of available data [18]) one can also get an idea about the general trend of the barrier and its change with the masses and charges of the interacting nuclei.

The results we obtain here for the value of the nuclear potential V_N at the barrier and its position R_B are summarized in the last two columns of table 3. Instead of trying to make a direct comparison with the experiment we found it more interesting to compare our results with those of Ngô *et al.* [7]), i.e. to compare the predictions of the Skyrme energy functional and the Brueckner energy density formalism for the interaction barrier. The consistency of our results with the experimental data will be discussed in the next section for the few cases for which we calculate the elastic scattering cross section.

In order to compare our results with those of Ngô *et al.* [7]) in fig. 8a we plot the quantity

$$r_B = R_B/(A_1^{\frac{1}{3}}+A_2^{\frac{1}{3}}), \tag{19}$$

as a function of $Z_1Z_2/(A_1^{\frac{1}{3}}+A_2^{\frac{1}{3}})$ and trace a curve between the calculated points to indicate the average trend of r_B. The corresponding curve from ref. [7]) is drawn on the same figure. One can see that both curves have the same trend but ours is situated by about 0.02 below that of Ngô *et al.*

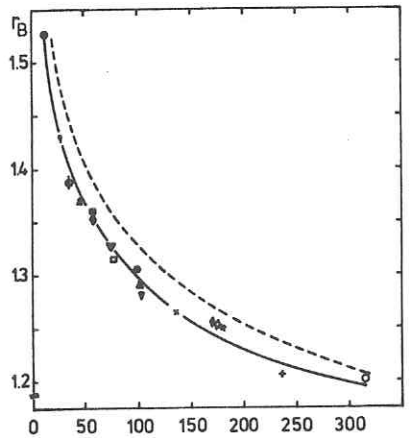

Fig. 8a. The quantity r_B from eq. (19) as a function of $Z_1Z_2/(A_1^{1/3}+A_2^{1/3})$. The full curve represents the average trend of r_B and is compared with the corresponding result of ref. [7]) broken curve). Pairs of nuclei are presented in the same way as in fig. 6.

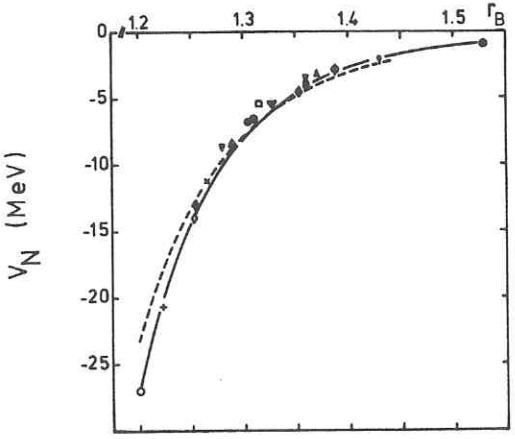

Fig. 8b. Same as fig. 8 but for V_N (nuclear potential at the barrier) versus r_B. Pairs of nuclei are represented in the same way as in fig. 6.

Another comparison suggested by ref. [7]) is shown in fig. 8b where the nuclear potential V_N at the top of the barrier is plotted as a function of r_B. For values of r_B around 1.33 our results for V_N are very near those of Ngô *et al.* But for lighter pairs of nuclei ($r_B > 1.4$) we get V_N slightly smaller than in ref. [7]) while for very heavy ions ($r_B < 1.25$) our values of V_N are in average ≈ 2 MeV below those of Ngô *et al.* There are two possible reasons for this difference. One is the functional itself. The other one could be the difference in the matter densities describing the nuclei. We found that for Skyrme energy functional the result is sensitive to changes in the density. If, for instance, we take trial densities for ^{16}O and ^{40}Ca with increased diffusivity parameters $a = 0.52$ and $a = 0.55$ respectively and find the other parameters by the normalization conditions (12) we obtain the barrier at the same position but $V_N(R_B) = -2.38$ MeV, i.e. lower by about 20%. These trial values of the diffusivity parameter might be nearer the true ones. As was mentioned before, the Skyrme interaction seems to give too steep a decrease of the density in the nuclear surface [11]).

4. Elastic scattering cross section

The purpose of this section is to show how well the calculated potential fits the elastic scattering data. We discuss only the elastic scattering of ^{16}O from different targets at several energies because for other projectiles we consider here like e.g. ^{40}Ca the experimental data are very scarce and less precise [19]). For the real part of the interaction we take a Woods-Saxon potential with parameters taken from table 3. By

TABLE 5

Comparison of calculated critical angle with the phenomenological value

Pair	E_{lab} (MeV)	W (MeV)	d^{cal} (fm)	θ_c^{cal} (deg)	θ_c^{exp} (deg)	V^{exp} (MeV)	R^{exp} (fm)	T^{exp} (fm)	W^{exp} (MeV)	R^{exp} (fm)	T_W^{exp} (fm)	Ref.
^{16}O+ ^{40}Ca	40	6.5	9.02	108	93	100	7.25	0.5	24.41	7.25	0.5	[21])
^{16}O+ ^{48}Ca	40	9.2	9.32	89	80.5	100	7.43	0.5	24.41	7.43	0.5	[21])
	60	10.5	9.25	45	42	32.8	8.00	0.5	8.11	8.00	0.5	[22])
^{16}O+^{208}Pb	104	13.4	12.06	86	79	40	11.06	0.45	15	11.06	0.45	[25])
^{16}O+ ^{30}Si	45	11.2	8.56	56.4	52	32.8	7.32	0.5	8.11	7.32	0.5	[22])
	60	11.11	8.52	37.2	36	32.8	7.32	0.5	14.0	7.03	0.5	[22])
	73.5	16.1	8.29	29.5	28	100	5.80	0.68	20.0	6.76	0.6	[23])
^{16}O+ ^{58}Ni	50	4.25	9.57	98	90	23.65	8.31	0.533	3.49	8.76	0.375	[24])
	60	8.4	9.56	68	63	25.25	8.31	0.533	5.39	8.76	0.375	[24])

Here, E_{lab} is the incident energy, W the adjusted strength of the imaginary part added to the calculated real part of the interaction potential (see text), θ_c^{cal} the calculated critical angle, θ_c^{exp} the phenomenological critical angle, and d^{cal} the calculated distance of closest approach (eq. (21)). The other columns quote

using the regularities found in the previous section the calculations of the elastic scattering cross sections can be extended to non-closed shell targets. We have calculated two examples, ^{16}O+^{30}Si and ^{16}O+^{58}Ni, for which there is good experimental data, using potential parameters given by formulae (16)–(18). In all cases we look at experimental angular distributions having a characteristic Fresnel diffraction pattern [20]). Hence the results are not very sensitive to the choice of the shape of the imaginary part of the optical potential. For this reason we take it to have the same geometry as the real part, and chose the strength W (table 5) to fit the value of the maximum peak in the ratio $\sigma(\theta)/\sigma_R(\theta)$ of the elastic cross section $\sigma(\theta)$ to the Rutherford cross section $\sigma_R(\theta)$.

Elastic scattering angular distributions have been calculated using the programme JIB3. It is difficult to compare with experimental data directly because of uncertainties in extracting the experimental values from published figures. We therefore chose to compare the scattering from our calculated potentials with the scattering produced by the Woods-Saxon potentials used in a phenomenological fit to the data. We have used a Coulomb interaction corresponding to a uniform charge distribution with radius R_C the same as that given by the phenomenological fit. The calculated scattering is insensitive to the choice of R_C.

The results for the pair ^{16}O+^{48}Ca are typical of most of the cases investigated. Fig. 9 shows that the cross section corresponding to the calculated potential has the same shape as the phenomenological one at two different incident energies; but that, in both cases, it is shifted to larger angles by a few degrees. A measure of this shift is given by the difference $\delta\theta_c = \theta_c^{cal} - \theta_c^{exp}$ between the critical angles for the calculated potential and the phenomenological one. By critical angle we

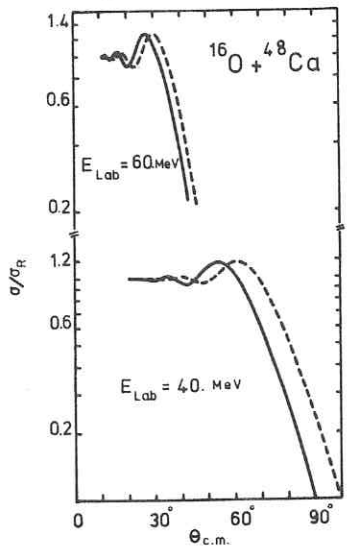

Fig. 9. Elastic scattering cross section for ^{16}O+^{48}Ca at E_{lab} = 40 and 60 MeV. The full curve is cal-

understand the angle for which $\sigma/\sigma_R = 0.25$. Values for the critical angles θ_c^{cal} and θ_c^{exp} for five different targets are given in table 5. This table also shows the parameters for the phenomenological potentials [21-25]).

Another quantity of interest is the distance of closest approach [20])

$$d = (\eta/\kappa)(1 + \operatorname{cosec} \tfrac{1}{2}\theta_c) \tag{20}$$

evaluated at the critical angle θ_c where κ is the relative wave number and η the dimensionless Coulomb parameter. This quantity (table 5) is a measure of the separation at which the interaction becomes important. A comparison between d and the sum of half-density radii $R_1 + R_2$ with R_i $(i = 1, 2)$ taken from table 2 indicates that the interaction becomes important at distances where the nuclei do not overlap too much. This shows the peripheral character of the elastic scattering process between heavy ions [2]) and supports the approximations made in eqs. (5) and (6).

From the results presented in table 5 we notice that the calculated critical angle is always a few percent larger than the experimental one. In other words, the "shadow" region of angular distribution is smaller than necessary and this suggests that the range of the calculated interaction potential is too small. The discrepancy $\delta\theta_c$ seems to be smaller in cases when θ_c is smaller. We can try to understand the variation of $\delta\theta_c$ with θ_c by using a sharp cut-off model [20]) where the interaction radius R_c is equal to d from formula (20). If the discrepancy $\delta\theta_c$ is due to a variation δR_c in R_c then by differentiating eq. (20) we get

$$\frac{\delta\theta_c}{\theta_c} = -\frac{1 + \sin \frac{1}{2}\theta_c}{\frac{1}{2}\theta_c \operatorname{ctg} \frac{1}{2}\theta_c} \frac{\delta R_c}{R_c}. \tag{21}$$

If θ_c is small then

$$\delta\theta_c/\theta_c \approx -\delta R_c/R_c, \tag{22}$$

while for larger angles $|\delta\theta_c/\theta_c| > |\delta R_c/R_c|$. For example if $\theta_c = 90°$ then

$$\delta\theta_c/\theta_c \approx -2.2\delta R_c/R_c. \tag{23}$$

This effect can be seen in the case of $^{16}O + ^{58}Ni$. At $E_{lab} = 50$ MeV the discrepancy $\delta\theta_c = 8°$ corresponds to a relative change in $\delta R_c/R_c = 0.041$ while at $E_{lab} = 60$ MeV the discrepancy $\delta\theta_c = 5°$ corresponds to $\delta R_c/R_c = 0.047$. The discrepancy $\delta\theta_c = 15°$ for the case $^{16}O + ^{40}Ca$ at $E_{lab} = 40$ MeV corresponds to $\delta R_c/R_c = 0.072$. The sharp cut-off radius R_c is almost equivalent to the barrier radius R_B in a potential model. Hence the discrepancy $\delta\theta_c = 15°$ corresponds to $\delta R_B = 0.61$ for $R_B = 8.5$ (cf. table 3). This change in R_B could be produced by a change in the potential radius $\delta R_0 \approx 0.6$. To test this estimates we have recalculated the angular distribution for $^{16}O + ^{40}Ca$ with a Woods-Saxon potential as in table 3 but with $R_0 = 7.4$. The resulting critical angle is $\theta_c \approx 93°$, like the phenomenological value.

5. Conclusions

By using the Skyrme energy density functional in the so called "sudden approximation" [5]) we have calculated the real part of the interaction potential between magic nuclei. As a result of the sudden approximation the potential has a repulsive core. The attractive part between the inflexion point and the barrier has a very similar shape to a Woods-Saxon potential, and for each pair of nuclei we found a Woods-Saxon potential with parameters which reproduce the calculated potential to within 1 %.

One of the purposes of parametrizing the tail of the potential with a Woods-Saxon shape was to look for regularities in the parameters with respect to the masses A_1 and A_2 of the colliding nuclei. Indeed it was found that all three parameters the depth V_0, the radius R_0 and the diffusivity T have a simple average dependence given by eqs. (16)–(18).

To check the validity of our results for the real part of the interaction potential we calculated the elastic scattering cross section for several pairs of nuclei. We chose cases where the absorption was strong so that the only significant part of the real potential was its tail. The absorption was taken into account by an imaginary potential with variable strength and the same geometry as the real part. In each case, we found that the grazing angle was somewhat larger than the experimental one.

The conclusion is that our potential gives too small a "shadow region" in the Fresnel diffraction pattern and this means that the real part of the potential has either too small a radius or too small a diffusivity (at fixed strength). This shortcoming might be due to the approximations explained in the text. On the other hand calculations of internuclear interactions based on Skyrme's force might have a deficiency related to the nature of the force. Skyrme's force is an effective interaction between nucleons in nuclei with parameters fitted to reproduce some bulk properties of nuclei such as binding energies and radii. The interaction potential in the barrier region is the result of the overlap of tails of nuclear density distributions where the total density is very small compared with nuclear matter densities. One might therefore question the validity of the present parametrization of Skyrme's interaction for such low densities.

The potentials derived here were obtained by a microscopic calculation from an effective density dependent nucleon-nucleon interaction. The purpose was to include saturation and exchange effects. The real parts of the potentials are determined completely from the calculation and there are no free parameters. When combined with a reasonable imaginary part a satisfactory fit to the elastic scattering data can be obtained for a wide range of pairs of nuclei. The potentials might not give an accurate enough fit to elastic scattering data to be used directly for calculating transfer reactions, etc., but this deficiency can be corrected by making a small increase in the radius parameter R_0 or the diffusivity T.

We would like to thank Dr. M. Beiner for providing us with Hartree-Fock

densities for magic nuclei before publication and Dr. D. Vautherin for giving us an opportunity to use his Hartree-Fock programme. Discussions with Drs. S. Kahana and C. Marty are gratefully acknowledged. One of us (Fl. S.) would like to thank Dr. P. E. Hodgson for offering to her very stimulating hospitality at the Nuclear Physics Department, Oxford.

References

1) D. M. Brink and N. Rowley, Nucl. Phys. **A219** (1974) 79
2) G. R. Satchler, Proc. Int. Conf. on reactions between complex nuclei, Nashville, 1974;
G. R. Satchler, Phys. Lett. **59B** (1975) 121
3) B. C. Sinha, Phys. Rev. Lett. **33** (1974) 600
4) H. Jaqaman and A. Z. Mekjian, Phys. Lett. **56B** (1975) 237
5) K. A. Brueckner *et al.*, Phys. Rev. **171** (1968) 1188; **181** (1969) 1543
6) J. D. Perez, Nucl. Phys. **A191** (1972) 19
7) C. Ngô *et al.*, Nucl. Phys. **A240** (1975) 353
8) H. Flocard, Phys. Lett. **49B** (1974) 129;
K. H. Pässler *et al.*, Phys. Lett. **47B** (1973) 419
9) D. M. Brink and Fl. Stancu, Nucl. Phys. **A243** (1975) 175
10) D. Vautherin and D. M. Brink, Phys. Rev. **C5** (1972) 626
11) M. Beiner *et al.*, Nucl. Phys. **A238** (1975) 29
12) M. Beiner, private communication
13) Y. M. Engel *et al.*, Nucl. Phys. **A249** (1975) 215
14) G. Reidemeister, Nucl. Phys. **A197** (1972) 631
15) J. P. Bondorf, I. M. Sobel and D. Sperber, Phys. Reports **15C** (1974) 83
16) J. Wilczyński and K. Siwek-Wilczyńska, Phys. Lett. **55B** (1975) 270
17) A. Bohr and B. R. Mottelson, Nuclear structure, vol. 1 (Benjamin, New York, 1969) p. 142
18) J. Galin *et al.*, Phys. Rev. **C9** (1974) 1018
L. C. Vaz and J. Alexander, Phys. Rev. **C10** (1974) 464
19) P. Colombani, preprint Orsay IPNO-Ph.N-74-09
20) D. M. Brink, Lecture notes on heavy-ion reactions, Orsay 1972
21) K. O. Groeneweld *et al.*, Phys. Rev. **C6** (1972) 805
22) J. B. Ball *et al.*, Nucl. Phys. **A244** (1975) 341
23) I. Tserruya *et al.*, Nucl. Phys. **A242** (1975) 345
24) P. R. Christensen *et al.*, Nucl. Phys. **A207** (1973) 433
25) F. D. Becchetti *et al.*, Phys. Rev. **C6** (1972) 2215